Inorganic Chemistry

ARTICLE

pubs.acs.org/IC

Ferrocene-Conjugated L-Tryptophan Copper(II) Complexes of Phenanthroline Bases Showing DNA Photocleavage Activity and Cytotoxicity

Tridib K. Goswami,[†] Balabhadrapatruni V. S. K. Chakravarthi,[‡] Mithun Roy,[†] Anjali A. Karande,*[,‡] and Akhil R. Chakravarty*[,†]

[†]Department of Inorganic and Physical Chemistry, Indian Institute of Science, Bangalore 560012, India

[‡]Department of Biochemistry, Indian Institute of Science, Bangalore 560012, India

Supporting Information

ABSTRACT: Ferrocene-conjugated L-tryptophan (L-Trp) reduced Schiff base (Fc-TrpH) copper(II) complexes [Cu(Fc-Trp)(L)](ClO$_4$) of phenanthroline bases (L), viz. 2,2′-bipyridine (bpy in **1**), 1,10-phenanthroline (phen in **2**), dipyrido[3,2-d:2′,3′-f]-quinoxaline (dpq in **3**), and dipyrido[3,2-a:2′,3′-c]phenazine (dppz in **4**), were prepared and characterized and their photocytotoxicity studied. Cationic reduced Schiff base (Ph-TrpH) complexes [Cu(Ph-Trp)(L)(H$_2$O)](ClO$_4$) (L = phen in **5**; dppz in **6**) having the ferrocenyl moiety replaced by a phenyl group and the Zn(II) analogue (**7**) of complex **4** were prepared and used as control species. The crystal structures of **1** and **5** with respective square-planar CuN$_3$O and square-pyramidal CuN$_3$O$_2$ coordination geometry show significantly different core structures. Complexes **1**−**4** exhibit a Cu(II)−Cu(I) redox couple near −0.1 V and the Fc$^+$−Fc couple at ∼0.5 V vs SCE in DMF−0.1 M [Bu$^n_4$N](ClO$_4$) (Fc = ferrocenyl moiety). The complexes display a copper(II)-based d−d band near 600 nm and a Fc-centered band at ∼450 nm in DMF−Tris-HCl buffer. The complexes are efficient binders to calf thymus DNA. They are synthetic chemical nucleases in the presence of thiol or H$_2$O$_2$, forming hydroxyl radicals. The photoactive complexes are cleavers of pUC19 DNA in visible light, forming hydroxyl radicals. Complexes **2**−**6** show photocytotoxicity in HeLa cancer cells, giving IC$_{50}$ values of 4.7, 10.2, 1.3, 4.8, and 4.3 μM, respectively, in visible light with the appearance of apoptotic bodies. The complexes also show photocytotoxicity in MCF-7 cancer cells. Nuclear chromatin cleavage has been observed with acridine orange/ethidium bromide (AO/EB) dual staining with complex **4** in visible light. The complexes induce caspase-independent apoptosis in the HeLa cells.

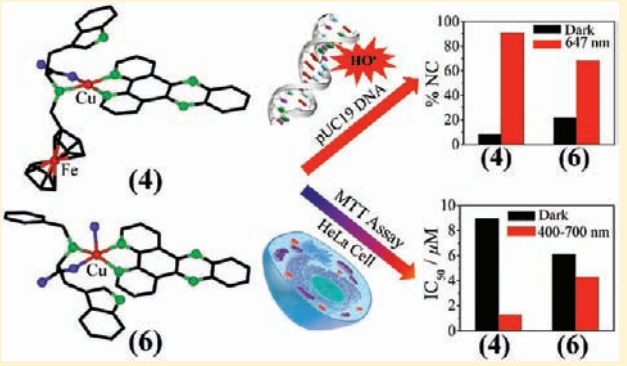

INTRODUCTION

Bioorganometallic chemistry is an emerging new discipline in chemical biology, and organometallic compounds are gaining continued importance as pharmaceuticals, bioprobes, tracers in nonisotropic immunoassay, and genosensors.[1−20] Design and evaluation of organometallic anticancer agents constitute an important area of interest, particularly to target both primary and metastatic secondary forms of tumors. Transition metal-based organometallic compounds have excellent biological activity, and such compounds are potent therapeutics for cancer, human retrovirus, malaria and fungal diseases and as radiopharmaceuticals and antibiotics. Among the different types of organometallic complexes, metallocenes and metal−arenes have been used as anticancer agents.[1,21−25] The ferrocene derivatives among the metallocenes are of importance for their stability in a biological medium and for their lipophilic, nontoxic, and reversible redox properties.[2,26] The cyclopentadienyl rings of ferrocene could be suitably functionalized, and ferrocenyl derivatives are known to exhibit antitumor, antimalarial, and antifungal properties. For example, the ferrocenyl moiety (Fc) in ferrocifen, the ferrocene-appended anticancer drug tamoxifen, makes the drug effective against both hormone-independent (ER−) and hormone-dependent (ER+) cells.[19] Similarly, ferroquine, the ferrocene-attached antimalarial drug chloroquine, is more effective than chloroquine.[20] Besides the ferrocene derivatives, ruthenium−arene and ruthenium−cyclopentadienyl half-sandwich complexes are known to show antitumor activity.[23−25]

The present work stems from our interest to develop the chemistry of ferrocenyl derivatives as photochemotherapeutic agents. The use of organometallic complexes in photodynamic therapy (PDT) is virtually unknown. PDT is a noninvasive therapeutic treatment of cancer in which the drug as a photosensitizer is photoactivated in the cancer cells using red light, thus generating reactive oxygen species (ROS) at the cancer cells, leaving the unexposed healthy cells unaffected from the cytotoxicity

Received: May 16, 2011
Published: July 28, 2011

Chart 1. Schematic Drawings of Complexes [Cu(Fc-Trp)(L)](ClO$_4$) (L = bpy, 1; phen, 2; dpq, 3; dppz, 4) and [Cu(Ph-Trp)(L)(H$_2$O)](ClO$_4$) (L = phen, 5; dppz, 6) and the Heterocyclic Bases Used

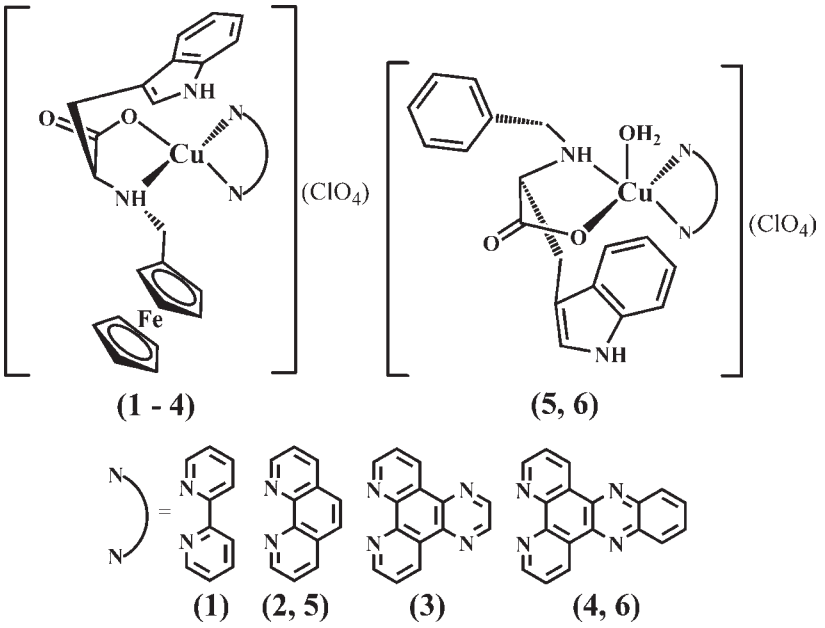

of ROS.[27−31] Porphyrin and phthalocyanine dyes have been extensively used as PDT agents. In contrast, organometallic complexes generally show photoinduced DNA cleavage activity in UV light.[32−34] Mohler and co-workers reported the photocleavage of pBR322 DNA by a cyclopentadienyl (Cp) complex [(Cp)W(CO)$_3$(CH$_3$)] using a light source of 450 W medium-pressure mercury arc lamp for 20 min via generation of methyl radicals.[33] Sheldrick and co-workers showed that pentamethylcyclopendienyl rhodium and iridium complexes of L-methionine methyl ester and dipyridophenazine photocleave plasmid DNA in UV light of 295 nm using a high-pressure 500 W Hg lamp.[34] Therrien and co-workers reported that porphyrin compounds having pendant (arene)ruthenium moieties show PDT effect with the organometallic units showing a chemotherapeutic effect while the porphyrin core displays photosensitizing activity in human Me300 melanoma cells in red light of 652 nm.[35] The UV-active nonporphyrinic organometallic complexes are not suitable for PDT applications since the basic requirement of red light for greater tissue penetration power than UV light is not fulfilled. This has prompted us to design nonporphyrinic organometallic conjugates of bioessential metal ions that could show visible light-induced DNA cleavage activity and photocytotoxicity.[36−39]

Recent reports from our laboratory have shown that ferrocene-conjugated copper(II) complexes are efficient photocleavers of DNA in red light. Complexes [Cu(L^1)(dpq/dppz)](ClO$_4$)$_2$ of ferrocenylmethylbis(2-pyridylmethylamine) (L^1 = FcCH$_2$N(CH$_2$Py)$_2$) and dipyridoquinoxaline (dpq) or dipyridophenazine (dppz) cleave supercoiled pUC19 DNA to its nicked circular form in red light of 647 nm via the hydroxyl radical pathway.[36] A similar DNA cleavage activity has been observed for analogous ferrocenyl−terpyridine copper(II) complexes having photoactive phenanthroline bases.[37] Amino acid L-methionine ferrocenyl reduced Schiff base copper(II) complexes also photocleave DNA in visible light.[38] The ferrocenyl moiety in these conjugates shows significant enhancement in the DNA photocleavage activity when compared to the control species that lack the ferrocenyl moiety. Considering the photosensitizing ability of L-tryptophan amino acid (L-Trp) and the potential of the indole moiety for noncovalent interactions with nucleic acids, we used the ferrocene-appended reduced Schiff base of L-tryptophan (Fc-TrpH) as a photosensitizer to prepare its copper(II) complexes having phenanthroline bases, viz. [Cu(Fc-Trp)(L)](ClO$_4$), where L is 2,2′-bipyridine (bpy in **1**), 1,10-phenanthroline (phen in **2**), dipyrido[3,2-d:2′,3′-f]quinoxaline (dpq in **3**), and dipyrido[3,2-a:2′,3′-c]phenazine (dppz in **4**) (Chart 1). To evaluate the potential of the ferrocenyl unit in photocleaving DNA, control complexes [Cu(Ph-Trp)(L)(H$_2$O)](ClO$_4$) (L = phen, **5**; dppz, **6**), where Ph-TrpH is the reduced Schiff base derived from benzaldehyde and L-tryptophan, are used. To study the presence of any cooperative effect between copper and the ferrocenyl moiety on the DNA cleavage activity, the zinc(II) analogue [Zn(Fc-Trp)(dppz)](ClO$_4$) (**7**) is prepared and used as a control species. Herein, we present the synthesis, structure, DNA binding property, DNA photocleavage activity, and photocytotoxicity of the complexes **1**−**7**. A significant result of this study is the enhancement in the DNA photocleavage activity of the ferrocene-appended copper(II) complexes in comparison to the control species. In addition, the ferrocenyl copper(II) complexes with steric protection of the axial sites from any ligand binding show no apparent hydrolytic cleavage of plasmid DNA, while the control species shows significant hydrolytic cleavage of DNA. Hydrolytic cleavage of DNA is undesirable for PDT since it results in dark toxicity. The photocytotoxic potential of the complexes has been evaluated in HeLa cells in visible light. The ferrocenyl copper(II) complex **4** of the dppz ligand shows a significant PDT effect in visible light via the apoptotic pathway.

EXPERIMENTAL SECTION

Materials and Measurements. All reagents and chemicals were obtained from commercial sources (s.d. Fine Chemicals, India; Aldrich)

dx.doi.org/10.1021/ic201028e |*Inorg. Chem.* 2011, 50, 8452–8464

and used as such. Solvents used were purified by reported procedures.[40] Supercoiled (SC) pUC19 DNA (cesium chloride purified) and DNase free RNase were purchased from Bangalore Genie (India). Tris-(hydroxymethyl)aminomethane-HCl (Tris-HCl) buffer solution was prepared using deionized and sonicated triple distilled water. Calf thymus (CT) DNA, agarose (molecular biology grade), distamycin, methyl green, catalase, 2,2,6,6-tetramethyl-4-piperidone (TEMP), ethidium bromide (EB), Hoechest 33258, acridine orange (AO), propidium iodide (PI), glutathione (GSH), and 3-mercaptopropionic acid (MPA) were from Sigma (USA). Dipyrido[3,2-d:2′,3′-f]quinoxaline (dpq) and dipyrido[3,2-a:2′,3′-c]phenazine (dppz) were prepared by reported literature procedures using 1,10-phenanthroline-5,6-dione as a precursor reacted with ethylenediamine and 1,2-phenylenediamine, respectively.[41,42]

Elemental analysis was carried out using a Thermo Finnigan Flash EA 1112 CHN analyzer. The infrared and electronic spectra were recorded on PerkinElmer Lambda 35 and PerkinElmer Spectrum one 55 spectrophotometers, respectively. ^{1}H NMR spectra were recorded at room temperature on a Bruker 400 MHz NMR spectrometer. Molar conductivity measurements were performed using a Control Dynamics (India) conductivity meter. Room-temperature magnetic susceptibility data were obtained from a George Associates Inc. Lewis-coil force magnetometer using Hg[Co(NCS)$_4$] as a standard. Experimental susceptibility data were corrected for diamagnetic contributions.[43] Cyclic voltammetric measurements were made at 25 °C on a EG&G PAR model 253 VersaStat potentiostat/galvanostat using a three-electrode setup comprising of a glassy carbon working, platinum wire auxiliary, and saturated calomel reference (SCE) electrode. Tetrabutylammonium perchlorate (TBAP) (0.1 M) was used as a supporting electrolyte in DMF. Electrochemical data were uncorrected for junction potentials. Electrospray ionization mass spectral measurements were done using an Esquire 3000 plus ESI (Bruker Daltonics) Spectrometer. Experimental and calculated ESI-MS values for each complex were identical to a significant last figure above the decimal point.

Synthesis of Fc-TrpH. L-Tryptophan (1.02 g, 5 mmol) and NaOH (0.2 g, 5 mmol) in dry methanol (10 mL) were stirred for 30 min to get a homogeneous solution. A methanol solution (10 mL) of ferrocenecarboxaldehyde (1.07 g, 5 mmol) was added dropwise to the above solution, which was refluxed for 90 min, cooled, and treated with sodium borohydride (0.38 g, 10 mmol) with constant stirring. The solvent was evaporated, the resulting mass was dissolved in water and acidified with dilute HCl, and the solution pH was maintained within 5−6. The ligand that precipitated as a yellow solid was filtered, thoroughly washed with water and cold methanol, and finally dried in vacuum over P_4O_{10} (yield 1.7 g, 85%) (Scheme S1, Supporting Information).

Anal. Calcd for $C_{22}H_{22}FeN_2O_2$: C, 65.69; H, 5.51; N, 6.93. Found: C, 65.41; H, 5.24; N, 6.98. ESI-MS in MeOH: m/z 425 [M + Na$^+$] (Figure S1, Supporting Information). IR (cm^{-1}): 1590vs (COO_{asym}), 1385vs $(COO)_{sym}$ (vs, very strong). ^{1}H NMR (400 MHz, D_2O): δ 7.69−7.71 (d, 1H, $^3J_{HH}$ = 7.8 Hz), 7.39−7.41 (d, 1H, $^3J_{HH}$ = 7.9 Hz), 7.09−7.18 (m, 3H), 4.06−4.10 (d, 4H), 3.87 (s, 5H), 3.43−3.46 (t, 1H, $^3J_{HH}$ = 6.7 Hz), 3.35−3.38 (d, 1H, $^2J_{HH}$ = 12.9 Hz), 3.13−3.16 (d, 1H, $^2J_{HH}$ = 12.9 Hz), 2.98−3.16 (m, 2H) (Figure S2, Supporting Information).

CAUTION! As the perchlorate salts are potentially explosive, only a small quantity of the complex was handled with precautions.

Synthesis of [Cu(Fc-Trp)(L)](ClO$_4$) (L = bpy, 1; phen, 2; dpq, 3; dppz, 4). Complexes **1**−**4** were prepared by a general synthetic procedure in which a 0.2 g (1.0 mmol) quantity of copper(II) acetate·hydrate in 15 mL of methanol was reacted with the heterocyclic base (L = bpy, 0.16 g; phen, 0.19 g; dpq, 0.23 g; dppz, 0.29 g; 1.0 mmol) while stirring at room temperature for 0.5 h followed by addition of solid Fc-TrpH (1.0 mmol, 0.4 g) in small portions with continuous stirring. The reaction mixture was stirred for 2 h, and the product was isolated as a green solid in ∼75% yield on addition of a methanol solution of NaClO$_4$ (1.0 mmol, 0.12 g). The solid was isolated, washed with water and cold methanol, and finally dried in vacuum over P_4O_{10} (yield 0.56 g, 78% for **1**; 0.55 g, 74% for **2**; 0.58 g, 73% for **3**; 0.60 g, 70% for **4**) (Scheme S2, Supporting Information).

Anal. Calcd for $C_{32}H_{29}ClCuFeN_4O_6$ (**1**): C, 53.35; H, 4.06; N, 7.78. Found: C, 53.17; H, 4.24; N, 7.71. ESI-MS in MeOH: m/z 620 [M − (ClO$_4^-$)]$^+$. UV−vis in DMF−Tris-HCl buffer (1:1 v/v) [λ_{max}, nm (ε, M^{-1} cm^{-1})]: 591 (100), 460sh (225), 276 (29 220), 264 (28 485). Selected IR data (cm^{-1}): 3515w, 3360w, 3145w, 2925w, 1650vs (COO_{asym}), 1450s, 1375s (COO_{sym}), 1340m, 1305m, 1255m, 1105vs (ClO$_4^-$), 920m, 815s, 755vs, 730s, 620vs, 500s, 480s, 420s (vs, very strong; s, strong; m, medium; w, weak).

Anal. Calcd for $C_{34}H_{29}ClCuFeN_4O_6$ (**2**): C, 54.85; H, 3.93; N, 7.53. Found: C, 54.59; H, 3.97; N, 7.35. ESI-MS in MeOH: m/z 644 [M − (ClO$_4^-$)]$^+$. UV−vis in DMF−Tris-HCl buffer (1:1 v/v) [λ_{max}, nm (ε, M^{-1} cm^{-1})]: 590 (120), 458sh (330), 271 (36 590). Selected IR data (cm^{-1}): 3585w, 3385br, 3250w, 3090w, 2930w, 1630vs (COO_{asym}), 1520m, 1340 m (COO_{sym}), 1430s, 1240w, 1080vs (ClO$_4^-$), 920w, 875w, 840s, 740s, 720s, 620vs, 480s, 430s (br, broad).

Anal. Calcd for $C_{36}H_{29}ClCuFeN_6O_6$ (**3**): C, 54.29; H, 3.67; N, 10.55. Found: C, 53.99; H, 3.50; N, 10.75. ESI-MS in MeOH: m/z 696 [M − (ClO$_4^-$)]$^+$. UV−vis in DMF−Tris-HCl buffer (1:1 v/v) [λ_{max}, nm (ε, M^{-1} cm^{-1})]: 587 (115), 455sh (405), 258 (43 240). Selected IR data (cm^{-1}): 3580w, 3385br, 3245w, 3090w, 2930w, 1635vs (COO_{asym}), 1490m, 1405s, 1385s (COO_{sym}), 1085vs (ClO$_4^-$), 815s, 730vs, 620vs, 485m, 425s.

Anal. Calcd for $C_{40}H_{31}ClCuFeN_6O_6$ (**4**): C, 56.75; H, 3.69; N, 9.93. Found: C, 56.56; H, 3.70; N, 10.15. ESI-MS in MeOH: m/z 746 [M − (ClO$_4^-$)]$^+$. UV−vis in DMF−Tris-HCl buffer (1:1 v/v) [λ_{max}, nm (ε, M^{-1} cm^{-1})]: 595 (120), 455sh (370), 377 (11 605), 360 (11 495), 276 (58 555). Selected IR data (cm^{-1}): 3584w, 3395w, 3245w, 3090w, 2925w, 1635s (COO_{asym}), 1500s, 1420s, 1355s (COO_{sym}), 1075vs (ClO$_4^-$), 815s, 765s, 730s, 655m, 620s, 480s, 425s.

Synthesis of Ph-TrpH. L-Tryptophan (0.4 g, 2 mmol) was initially dissolved in dry methanol (20 mL) on addition of NaOH (0.08 g, 2 mmol) with continuous stirring. Benzaldehyde (0.2 mL, 2 mmol) was subsequently added to the above solution. The mixture was refluxed for 60 min, cooled, and then treated with an excess of solid NaBH$_4$ with constant stirring. After stirring for ∼15 min, the solvent was removed and the resulting mass was dissolved in water followed by treatment with dilute HCl to maintain a pH of ∼5.5. A white solid thus precipitated was filtered off, thoroughly washed with water and cold methanol, and finally dried in vacuum over P_4O_{10} (Yield: 0.48 g, 82%) (Scheme S1, Supporting Information).

Anal. Calcd for $C_{18}H_{18}N_2O_2$: C, 73.45; H, 6.16; N, 9.52. Found: C, 73.17; H, 6.10; N, 9.78. ESI-MS in MeOH: m/z 317 [M + 23(Na$^+$)] (Figure S3, Supporting Information). IR (cm^{-1}): 1595vs (COO_{asym}), 1395vs $(COO)_{sym}$. ^{1}H NMR (400 MHz, D_2O): δ 7.45−7.47 (d, 1H, $^3J_{HH}$ = 8 Hz), 7.29−7.31 (d, 1H, $^2J_{HH}$ = 8 Hz), 6.92−7.19 (m, 8H), 3.56−3.59 (d, 1H, $^2J_{HH}$ = 12.9 Hz), 3.37−3.40 (d, 1H, $^2J_{HH}$ = 12.8 Hz), 3.25−3.28 (t, 1H, $^3J_{HH}$ = 6.8 Hz), 2.85−2.95 (m, 2H) (Figure S4, Supporting Information).

Synthesis of [Cu(Ph-Trp)(L)(H$_2$O)](ClO$_4$) (L = phen, 5; dppz, 6). Complexes **5** and **6** were synthesized following a similar procedure as described for complexes **1**−**4** (1.0 mmol scale). The complexes were isolated as a dark blue solid (yield 0.49 g, 75% for **5**; 0.55 g, 73% for **6**) (Scheme S3, Supporting Information).

Anal. Calcd for $C_{30}H_{25}ClCuN_4O_7$ (**5**): C, 55.05; H, 4.16; N, 8.56. Found: C, 54.83; H, 4.17; N, 8.52. ESI-MS in MeOH: m/z 536 [M − (H$_2$O + ClO$_4^-$)]$^+$. UV−vis in DMF−Tris-HCl buffer (1:1 v/v) [λ_{max}, nm (ε, M^{-1} cm^{-1})]: 603 (100), 271 (32 840). IR data (cm^{-1}): 3540w, 3365 m, 3255w, 2925m, 1740m, 1635vs (COO_{asym}), 1520m, 1455m, 1425s, 1380s (COO_{sym}), 1345m, 1215m, 1070vs (ClO$_4^-$), 980m, 835s, 745s, 720s, 620s, 560 m, 455w, 425s.

Anal. Calcd for $C_{36}H_{29}ClCuN_6O_7$ (**6**): C, 57.14; H, 3.86; N, 11.11. Found: C, 56.85; H, 3.97; N, 11.21. ESI-MS in MeOH: m/z 638

Table 1. Selected Crystallographic Data for Complexes [Cu(Fc-Trp)(bpy)](ClO_4)·H_2O (1·H_2O) and [Cu(Ph-Trp)(phen)](ClO_4) (5)

	1·H_2O	5
empirical formula	$C_{32}H_{31}ClCuFeN_4O_7$	$C_{30}H_{27}ClCuN_4O_7$
fw, g M^{-1}	738.45	654.55
cryst syst	orthorhombic	Orthorhombic
space group	$P2_12_12_1$	$P2_12_12_1$
a, Å	9.665(3)	10.9338(6)
b, Å	14.257(4)	12.0549(6)
c, Å	22.127(6)	22.5692(12)
α, deg	90	90
β, deg	90	90
γ, deg	90	90
V, $Å^3$	3048.8(15)	2974.8(3)
Z	4	4
T, K	293(2)	293(2)
ρ_{calcd}, g cm^{-3}	1.609	1.461
λ, Å (Mo Kα)	0.71073	0.71073
μ, mm^{-1}	1.314	0.877
data/restraints/parameters	7136/0/539	8984/0/388
F(000)	1516	1196
goodness-of-fit	0.996	0.993
R (F_o)[a], $I > 2\sigma(I)$ [wR (F_o)[b]]	0.0320 [0.0683]	0.0381 [0.0920]
R (all data) [wR (all data)]	0.0450 [0.0720]	0.0962 [0.1202]
largest diff. peak and hole (e $Å^{-3}$)	0.392, −0.190	0.475, −0.344

[a] $R = \Sigma||F_o| - |F_c||/\Sigma|F_o|$. [b] $wR = \{\Sigma[w(F_o^2 - F_c^2)^2]/\Sigma[w(F_o)^2]\}^{1/2}$; $w = [\sigma^2(F_o)^2 + (AP)^2 + BP]^{-1}$, where $P = (F_o^2 + 2F_c^2)/3$, $A = 0.0397$ and $B = 0.0000$ for 1·H_2O and $A = 0.0571$ and $B = 0.6475$ for **5**.

$[M - (H_2O + ClO_4^-)]^+$. UV−vis in DMF−Tris-HCl buffer (1:1 v/v) [λ_{max}, nm (ε, M^{-1} cm^{-1})]: 585 (124), 377 (12 635), 360 (13 035), 276 (63 400). IR data (cm^{-1}): 3433br, 3237w, 3063w, 2943w, 1645vs (COO_{asym}), 1607s, 1498m, 1448m, 1422m, 1385m (COO_{sym}), 1342m, 1236m, 1211w, 1090vs (ClO_4^-), 985s, 932m, 820s, 745s, 703m, 620s, 458s, 555m, 425s.

Synthesis of [Zn(Fc-Trp)(dppz)](ClO_4) (7). Complex **7** was prepared from a reaction of zinc(II) nitrate.hydrate (0.3 g, 1.0 mmol) in 5 mL of methanol with a methanolic solution of Fc-TrpH (1.0 mmol, 0.4 g) at room temperature for 1 h stirring followed by addition of a methanolic solution of dppz (0.29 g; 1.0 mmol). The product was isolated as a yellow solid in ∼70% yield on addition of a methanol solution of $NaClO_4$ (1.0 mmol, 0.12 g). The solid was washed with water and cold methanol and finally dried in vacuum over P_4O_{10} (yield 0.60 g, 71%).

Anal. Calcd for $C_{40}H_{31}ClFeZnN_6O_6$ (**7**): C, 56.63; H, 3.68; N, 9.91. Found: C, 56.32; H, 3.41; N, 9.72. ESI-MS in MeOH: m/z 747 $[M - (ClO_4^-)]^+$. UV−vis in DMF−Tris-HCl buffer (1:1 v/v) [λ_{max}, nm (ε, M^{-1} cm^{-1})]: 440 (490), 380 (23 070), 360 (22 095), 270 (95 000). IR data (cm^{-1}): 3215w, 3085br, 2925w, 2288w, 2210w, 2180w, 2112w, 2055w, 1990w, 1925w, 1590s (COO_{asym}),1495m, 1420s (COO_{sym}), 1355m, 1235w, 1080vs (ClO_4^-), 910w, 817m, 738s, 620m, 580w, 488m, 425m.

Solubility and Stability. The complexes were soluble in MeOH, DMF, DMSO, and MeCN, less soluble in $CHCl_3$ and CH_2Cl_2, and insoluble in hydrocarbon solvents. The complexes were stable in both solid and solution phases. The stability of complex **2** in a solution phase (DMF−Tris-HCl buffer, 1:1 v/v) was studied by monitoring its UV−vis absorption bands and the cyclic voltammetric redox couples over a period of 12 h. There was no apparent change in the spectral and redox properties, suggesting solution stability of the complex (Figure S5, Supporting Information).

X-ray Crystallographic Procedure. The crystal structures of [Cu(Fc-Trp)(bpy)](ClO_4)·H_2O (1·H_2O) and [Cu(Ph-Trp)(phen)(H_2O)](ClO_4) (**5**) were obtained by the single-crystal X-ray diffraction method. Crystals of 1·H_2O and **5** were isolated from methanol solutions of the complexes on slow evaporation of the solvent. Crystal mounting was done on a glass fiber with epoxy cement. All geometric and intensity data were collected at room temperature using an automated Bruker SMART APEX CCD diffractometer equipped with a fine-focus 1.75 kW sealed tube Mo Kα X-ray source (λ = 0.71073 Å) with increasing ω (width of 0.3° per frame) at a scan speed of 5 s per frame. Intensity data, collected using an $\omega-2\theta$ scan mode, were corrected for Lorentz−polarization effects and absorption.[44] Structure solution was done by the combination of Patterson and Fourier techniques and refined by full-matrix least-squares method using the SHELX system of programs.[45] Hydrogen atoms belonging to the complex were in their calculated positions and refined using a riding model. The non-hydrogen atoms were refined anisotropically. Selected crystallographic data are given in Table 1. The perspective views of the molecules were obtained using ORTEP.[46] The lattice water in the crystal structure of 1·H_2O showed a hydrogen-bonding interaction with one perchlorate anion oxygen atom, a carboxylate oxygen atom, and the NH proton of the amino acid reduced Schiff base ligand (Figure S6, Supporting Information).

DNA Binding Methods. The absorption spectral and viscosity experiments were carried out in 5 mM Tris-HCl buffer (pH 7.2) at an ambient temperature. The DNA melting experiments were performed using phosphate buffer (pH 6.8). The ratio of the absorbance values of CT DNA at 260 and 280 nm in Tris-HCl buffer was found to be 1.9:1, indicating the DNA is free from any protein impurities. The DNA concentration in the base pair was determined by absorption spectroscopy using a molar absorption coefficient value of 6600 M^{-1} cm^{-1} at 260 nm for calf thymus (CT) DNA.[47] In the UV−vis absorption titration experiment using the spectral band at ∼260 nm, the complex solution (40 μM) in DMF was titrated with 220 μM CT DNA. Due correction was made for the absorption of DNA itself. The spectra were recorded after equilibration for 5 min, allowing the complexes to bind to the CT DNA. The intrinsic equilibrium binding constant (K_b) and the fitting parameter (s) of the complexes to CT DNA were obtained by the McGhee−von Hippel (MvH) method using the expression of Bard and co-workers.[48,49]

DNA thermal denaturation studies were carried out by monitoring the absorption intensity of CT DNA (190 μM) at 260 nm by varying the temperature from 40 to 90 °C at a rate of 0.5 °C/min in both the absence and the presence of complexes **1**−**7** (20 μM) with a complex to CT DNA molar ratio of 1:9.5 using a Cary 300 bio UV−visible spectrometer having a Cary temperature controller. Viscometric titration experiments were performed using a Schott Gerate AVS310 Automated Viscometer that was thermostatted at 37(±0.1) °C in a constant temperature bath. The concentration of CT DNA was 160 μM. The flow time was measured with an automated timer. The data were presented by plotting the relative specific viscosity of DNA $(\eta/\eta_0)^{1/3}$ vs [complex]/[DNA], where η is the viscosity of DNA in the presence of the complex and η_0 is the viscosity of DNA alone in 5 mM Tris-HCl buffer medium. The viscosity values were calculated from the observed flow time of CT DNA containing solutions (t) duly corrected for that of the buffer alone (t_0), $\eta = (t - t_0)/t_0$.[50]

DNA Cleavage Experiments. Cleavage of supercoiled pUC19 DNA (30 μM, 0.2 μg, 2686 base pairs) was studied by agarose gel electrophoresis using metal complexes in 50 mM tris(hydroxymethyl)-methane-HCl (Tris-HCl) buffer (pH 7.2) containing 50 mM NaCl. The chemical nuclease activity of the complexes was studied using hydrogen peroxide as an oxidizing agent and 3-mercaptopropionic acid (MPA) or glutathione (GSH) as the reducing agent. The DNA photocleavage

reactions were carried out in visible light at wavelengths of 454, 568, and 647 nm using a Spectra Physics Water-Cooled Mixed-Gas Ion Laser Stabilite 2018-RM (continuous-wave (CW) beam diameter at $1/e^2$ 1.8 mm ±10% and beam divergence with full angle 0.7 mrad ± 10%). The laser beam power at the sample position (5 cm from the aperture with a solution path length of 5 mm) was 50 mW, measured using a Spectra Physics CW Laser Power Meter (model 407A). After light exposure, each sample was incubated for 1.0 h at 37 °C and analyzed for the photocleaved products using gel electrophoresis following procedures reported earlier.[51] The mechanistic studies were carried out using different additives as quenchers of singlet oxygen (NaN_3, 1.0 mM; TEMP, 1.0 mM) and scavengers of hydroxyl radicals (DMSO, 4 μL; KI, 1.0 mM; mannitol, 1.0 mM; catalase, 4 units) prior to addition of the complex. The extent of DNA cleavage was calculated from the intensities of the bands using the UVITEC Gel Documentation System. Due corrections were made for the low level of nicked circular form present in the original supercoiled DNA sample and for the low affinity of EB binding to supercoiled compared to nicked circular and linear forms of DNA.[52] The concentrations of the complexes and additives corresponded to that in the 20 μL final volume of the sample using Tris buffer.

Cell Viability Assay. The photocytotoxicity of the complexes was assessed using MTT assay based on the ability of mitochondrial dehydrogenases in the viable cells to cleave the tetrazolium rings of MTT and forming dark blue membrane-impermeable crystals of formazan that could be measured at 595 nm.[53] The formazan product formed gave a measure of the number of viable cells. Approximately 15 000 cells of human cervical carcinoma HeLa or 20 000 cells of MCF-7 (human breast adenocarcinoma) were plated in a 96-well culture plate in DMEM supplemented with 10% fetal bovine serum. After 24 h of incubation of the sample at 37 °C in a CO_2 incubator, different concentrations of the phen and dppz complexes (0.1, 0.5, 1, 5, 10, and 20 μM each) were added to the cells, and incubation was continued for 4 h in the dark. After incubation, the medium was replaced with PBS and photoirradiated for 1.0 h in visible light of 400−700 nm using a Luzchem Photoreactor (model LZC-1, Ontario, Canada; light fluence rate = 2.4 mW cm^{-2}; light dose = 10 J cm^{-2}). PBS was replaced with 10% DMEM after irradiation. Incubation was continued for a further period of 20 h in the dark following which 20 μL of 5 mg mL^{-1} of MTT was added to each well and incubated for an additional 3 h. The culture medium was discarded, and 100 μL of DMSO was added to dissolve the formazan crystals. The absorbance at 595 nm was determined using an ELISA microplate reader (BioRad, Hercules, CA). The cytotoxicity of the test compounds was measured as the percentage ratio of the absorbance of the treated cells over the untreated controls. The IC_{50} values were determined by nonlinear regression analysis (GraphPad Prism).

Cell Cycle Analysis. HeLa cells were seeded in 24-well plates in 10% DMEM at a density of 0.25 × 10^6 cells per well. After overnight adherence, the cells were pretreated with 50 μM of cell-permeable Z-VAD-FMK (pan caspase inhibitor) for 1 h. The cells were further cultured in 5 μM of each complex, namely, **2**, **4**, **5**, and **6**, and incubation was continued for 4 h in the dark. After incubation, the medium was replaced with PBS and photoirradiated for 1 h, and the procedure adopted was as given for a cell viability assay.[54] HeLa cells were centrifuged at 300*g* for 5 min, taken in 100 μL of 50 mM phosphate-buffered saline (PBS), and fixed with ice-cold 70% (v/v) ethanol for 30 min at −20 °C. The cells were pelleted, washed once with PBS, stained with DNA staining solution containing 20 μg mL^{-1} propidium iodide and 20 μg mL^{-1} DNase free RNase in PBS, and subjected to flow cytometry (FACS caliber, BD Biosciences, USA). The percentages of cells in sub G1 phase were analyzed with CellQuest Pro software using an excitation 488 nm laser and emission at 560/670 nm.[55] A minimum of 10 000 cells were acquired per sample, and the histograms were analyzed using WinMDI 2.9 software.

Fluorescence Microscopy of HeLa Cells with Complex 4. The changes in chromatin organization following photoexposure after treatment with complex **4** were determined microscopically by assessing staining with Hoechst 33258 and an acridine orange/ethidium bromide (AO/EB) dual stain. Hoechst staining was performed by a published procedure.[56] Briefly, about 2 × 10^4 cells were allowed to adhere overnight on a 25 mm coverslip placed in each well of 24-well plate. The control and cells were treated with complex **4** (10 μM) for 4 h in the dark, followed by irradiation with visible light of 400−700 nm (10 J cm^{-2}) for 1 h. They were fixed with 4% (v/v) paraformaldehyde in PBS (pH 7.4) for 10 min at room temperature, permeabilized with 0.1% Triton X-100 for 10 min, and stained with Hoechst 33258 (1 mg mL^{-1} in PBS) for 5 min. After being washed twice with PBS, cells were examined by fluorescence microscopy (360/40 nm excitation and 460/50 nm emission filters). The apoptotic cells were identified by the presence of highly condensed or fragmented nuclei. The protocol for AO/EB that was used was derived from the reported ones.[57] The cells were allowed to recover for 1 h, washed thrice with PBS, stained with an AO/EB mixture (1:1, 10 μM) for 15 min, and observed at 10× magnification with a fluorescence microscope using 485/20 nm excitation and 535/40 nm emission filter sets.

RESULTS AND DISCUSSION

Synthesis and General Aspects. Ferrocene-conjugated ternary copper(II) complexes [Cu(Fc-Trp)(L)](ClO_4) (**1**−**4**) having N,N-donor heterocyclic bases (L = bpy, **1**; phen, **2**; dpq, **3**; dppz, **4**) were prepared in good yield (∼80%) from reaction of ferrocenylmethyltryptophan (Fc-TrpH) with copper(II) acetate monohydrate and the respective phenanthroline base in methanol (Chart 1). To explore the effect of the ferrocenyl moiety on the overall DNA cleavage activity and photocytotoxicity of **1**−**4**, complexes [Cu(Ph-Trp)(L)(H_2O)](ClO_4) with L as phen (in **5**) and dppz (in **6**) were prepared, where Ph-TrpH is the reduced Schiff base derived from benzaldehyde and L-tryptophan. Further, to investigate the concerted mechanism involved, if any, between the Fe(II) and the Cu(II) centers in the ferrocene conjugates, a Zn(II) analogue of **4**, namely, [Zn(Fc-Trp)(dppz)](ClO_4) (**7**) was prepared and studied as a control species. The complexes were characterized by various spectroscopic and analytical methods (Table 2). The ESI MS spectra of the complexes showed an essentially single peak assignable to the cationic complex $[M - ClO_4]^+$ (Figures S7−S13, Supporting Information). The IR spectra of the complexes displayed characteristic stretching bands near 1650 and 1350 cm^{-1} due to asymmetric and symmetric COO along with the ClO_4^- band at ∼1080 cm^{-1}.[58] The complexes were 1:1 electrolytic in DMF, giving a molar conductance value of ∼80 S m^2 M^{-1} at 25 °C. The magnetic moment values of ∼1.8 μ_B for **1**−**6** at 25 °C suggest the presence of one-electron paramagnetic $3d^9$ copper(II) centers in these copper(II) conjugates. The UV−vis spectra of **1**−**4** in DMF−Tris-HCl buffer (1:1 v/v) displayed a broad and weak copper-centered d−d band in the range of 585−605 nm (Figure 1, Figure S14, Supporting Information). A ferrocene-centered visible band was observed near 440 nm.[59] The ligand-based electronic transitions were observed in the UV region. The bands observed near 370 nm in **4** could be due to dppz ligand showing $n-\pi^*$ transitions.[60] Complexes **1**−**4** were redox active and displayed a quasi-reversible cyclic voltammetric response near 0.5 V vs SCE in DMF−0.1 M TBAP assignable to the Fc^+−Fc couple, where Fc is the ferrocenyl moiety (Table 2, Figure 1). There is a significant positive shift of ∼70 mV in the

Table 2. Selected Physicochemical Data for Complexes [Cu(Fc-Trp)(L)](ClO$_4$) (L = bpy, 1; phen, 2; dpq, 3; dppz, 4), [Cu(Ph-Trp)(L)(H$_2$O)](ClO$_4$) (L = phen, 5; dppz, 6), and [Zn(Fc-Trp)(dppz)](ClO$_4$) (7)

			E_f/V (ΔE_p /mV)[b]			
complex	IR/cm^{-1} [ν (ClO$_4^-$)]	λ_{max}/nm (ε/M^{-1} cm^{-1})[a]	Fc$^+$−Fc	Cu(II)−Cu(I)	Λ_M[c]/S m^2 M^{-1}	μ_{eff}[d]/μ_B
1	1105	460 (225), 591 (100)	0.51 (90)	−0.16 (440)	81	1.79
2	1080	458 (330), 590 (120)	0.51 (90)	−0.16 (450)	78	1.81
3	1085	455 (405), 587 (115)	0.50 (100)	−0.17 (450)	80	1.80
4	1075	455 (370), 595 (120)	0.49 (100)	−0.18 (470)	80	1.80
5	1070	603 (100)		−0.16 (340)	77	1.78
6	1090	585 (124)		−0.13 (420)	79	1.80
7	1080	440 (490)	0.42 (100)		78	-

[a] In DMF−Tris-HCl buffer (1:1 v/v). The bands near 450 and 600 nm are ferrocene based and Cu(II) based, respectively. [b] Fc$^+$−Fc and Cu(II)−Cu(I) redox couple in DMF−0.1 M TBAP, $E_f = 0.5(E_{pa} + E_{pc})$, $\Delta E_p = (E_{pa} - E_{pc})$, where E_{pa} and E_{pc} are the anodic and cathodic peak potentials, respectively. The potentials are vs SCE. Scan rate = 50 mV s^{-1}. [c] Molar conductivity in DMF. [d] Magnetic moment at 298 K using solid powdered samples of the complexes.

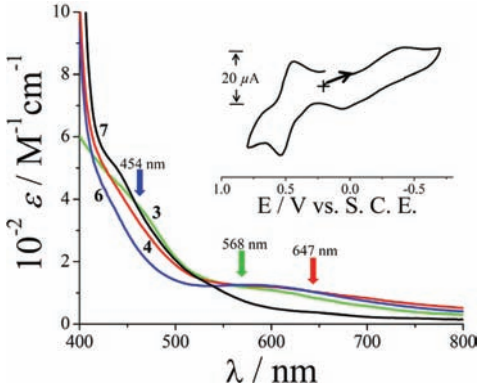

Figure 1. Electronic spectra of [Cu(Fc-Trp)(L)](ClO$_4$) (L = dpq, **3**, green; dppz, **4**, red), [Cu(Ph-Trp)(dppz)(H$_2$O)](ClO$_4$) (**6**, blue), and [Zn(Fc-Trp)(dppz)](ClO$_4$) (**7**, black) in DMF−Tris-HCl buffer (1:1 v/v). The arrows show the laser wavelengths used for the DNA photocleavage study. (Inset) Cyclic voltammetric responses of complex **4** in DMF−0.1 M TBAP (scan rate 50 mV s^{-1}).

Fe(III)−Fe(II) potential in these complexes compared to that of only ferrocene (0.43 V vs SCE). The copper(II) complexes also showed a quasi-reversible cyclic voltammetric response near −0.15 V assignable to the Cu(II)−Cu(I) redox couple (Figures S15 and S16(a), Supporting Information). Complex **7** displayed the Fc$^+$−Fc redox couple near 0.4 V vs SCE in DMF−0.1 M TBAP (Figure S16(b), Supporting Information). Ligand reductions were observed near −1.1 and −1.7 V in these complexes.

Crystal Structure. Complexes **1**·H$_2$O and **5** were structurally characterized by single-crystal X-ray diffraction. The complexes crystallized in the $P2_12_12_1$ space group in the orthorhombic crystal system with four molecules in the unit cell. The ORTEP views of the complexes are shown in Figure 2 (unit cell packing diagrams in Figures S17 and S18, Supporting Information). The structure of **1**·H$_2$O consists of a discrete heterobimetallic complex having Cu(II) and Fe(II) centers. The crystal structure shows a square-planar geometry of the Cu(II) center with a CuN$_3$O coordination (τ = 0.032) with both axial sites being sterically protected by two pendant groups of Fc-Trp.[61] The monoanionic Fc-Trp having a covalently linked ferrocenyl moiety shows a bidentate N,O-coordination mode to the copper(II) with the indole ring of tryptophan blocking one axial coordination site. The other axial site is blocked by the pendant ferrocenyl unit. The heterocyclic ligand shows a bidentate mode of binding to the copper(II) center with Cu−N bond distances of 1.975(2) and 2.007(2) Å (Table S1, Supporting Information). The cyclopentadienyl (Cp) rings in the Fc moiety are in an eclipsed conformation. The dihedral angle between the η^5-C$_5$H$_5$ and the η^5-C$_5$H$_4$ rings is 2.8°. The average Fe−C bond distance is 2.039 Å. The chiral carbon of L-tryptophan has the "*S*" configuration.

The structure of complex **5** consists of a copper(II) center having a distorted square-pyramidal geometry with a CuN$_3$O$_2$ core (τ value = 0.22).[61] The anionic Ph-Trp ligand provides a different steric environment to the Cu(II) center than Fc-Trp with the phenyl ring positioning itself away from the axial coordination site that is occupied by an aqua ligand. The indole unit of tryptophan blocks one axial site in a similar way as that observed in the structure of complex **1**. The Cu−N bond distances are in the range of 2.015(3)−2.047(2) Å (Table S2, Supporting Information). A comparison of the crystal structures reveals that the ferrocene moiety in **1** induces significant structural differences by stabilizing the square-planar geometry, while a square-pyramidal structure is observed for complex **5**. The ferrocenyl complexes having the axial sites blocked by the indole ring and the ferrocenyl moiety are likely to impart greater structural stability than the control species in which the axial aqua ligand bound to the Lewis acidic copper(II) could facilitate the undesirable hydrolytic cleavage of DNA by targeting the phosphodiester linkage.

DNA Binding Property. The binding property of the complexes to calf-thymus (CT) DNA was studied using spectral, DNA melting, and viscometric methods (Table 3). The equilibrium binding constants (K_b) of the complexes to CT-DNA were obtained from UV−vis absorption titration experiments by monitoring the change in the absorption intensity of the ligand-centered band of the complexes at ∼270 nm. Significant hypochromicity along with a minor bathochromic shift of this band is observed, suggesting a primarily groove binding nature of the complexes to CT DNA in Tris-HCl buffer medium (Figure S19, Supporting Information). Small molecules that are known to π stack between two DNA base pairs are DNA intercalators that show a much larger bathochromic shift and hypochromism of the spectral bands.[62] The K_b values of complexes **2**−**7** are in the range from 1.89(±0.11) × 10^5 to 1.67(±0.13) × 10^6 M^{-1}

dx.doi.org/10.1021/ic201028e |*Inorg. Chem.* 2011, 50, 8452–8464

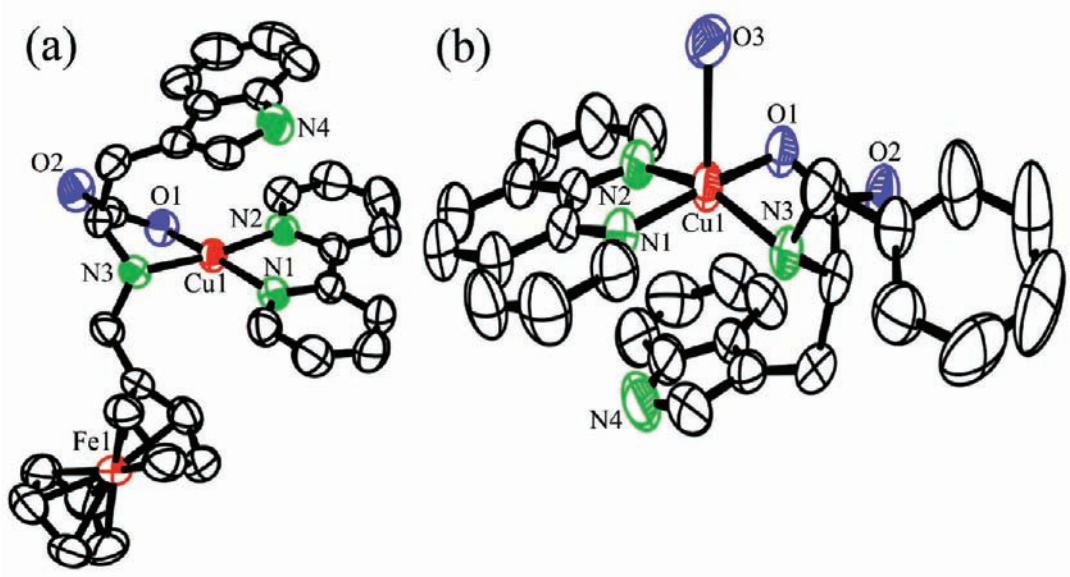

Figure 2. ORTEP views of the cationic complexes in $[Cu(Fc\text{-}Trp)(bpy)](ClO_4)\cdot H_2O$ (**1**$\cdot H_2O$) (a) and $[Cu(Ph\text{-}Trp)(phen)(H_2O)](ClO_4)$ (**5**) (b) showing 50% probability thermal ellipsoids and the atom-numbering scheme for the metal and heteroatoms. The hydrogen atoms are omitted for clarity. Atoms color code: Fe and Cu, red; O, blue; N, green; C, black.

Table 3. DNA Binding Data for Complexes $[Cu(Fc\text{-}Trp)(L)](ClO_4)$ (L = phen, 2; dpq, 3; dppz, 4), $[Cu(Ph\text{-}Trp)(L)(H_2O)](ClO_4)$ (L = phen, 5; dppz, 6), and $[Zn(Fc\text{-}Trp)(dppz)](ClO_4)$ (7)

	2	3	4	5	6	7
$K_b{}^a/M^{-1}$ [s]	1.89 (±0.11) $\times 10^5$ [0.07]	1.09(±0.57) $\times 10^6$ [0.17]	1.67(±0.13) $\times 10^6$ [0.21]	2.05(±0.10) $\times 10^5$ [0.08]	1.28(±0.58) $\times 10^6$ [0.20]	1.61(±0.29) $\times 10^6$ [0.20]
$\Delta T_m{}^b$ /°C	2.4	4.2	5.5	2.1	5.1	5.2

[a] Intrinsic equilibrium CT DNA binding constant from UV−vis absorption spectral experiments. [b] Change in CT DNA melting temperature.

giving an order **4** ≈ **7** > **6** > **3** > **2** ≈ **5** (Table 3).[48,49] The planar phenazine ring of the dppz ligand seems to have facilitated partial intercalation of this base through the DNA groove, resulting in a higher binding strength of **4**, **6**, and **7** than their dpq or phen analogues. The low value of the fitting parameter (*s*) suggests the groove-binding nature of the complexes to the duplex DNA in preference to intercalation.[63]

The DNA melting experiments were carried out to investigate the effect of DNA duplex stability due to binding of the complexes. Duplex DNA at its melting temperature unwinds to give single-strand DNA, thus increasing its absorbance at 260 nm. The DNA intercalator ethidium bromide (EB) stabilizes the duplex DNA to a significant extent, causing DNA to melt at a significantly higher temperature.[64] Complexes **1**−**7** have comparatively lower values of ΔT_m ranging within 2.1−5.5 °C than ethidium bromide (ΔT_m = 13 °C), indicating primarily DNA groove-binding property of the complexes (Figure 3a). The dppz complex with a relatively high ΔT_m value of 5.5 °C could have a partial intercalative mode of binding to DNA. In contrast, the bpy complex **1** does not change the melting temperature, suggesting no stabilizing effect of this complex on the double-stranded DNA. Viscometric titration experiments were done to determine the relative specific viscosity of CT DNA in the presence of the complexes. Again, an intercalator like ethidium bromide shows a significant increase in the relative viscosity of the CT DNA solution due to an increase in the overall DNA contour length on binding to DNA.[65] DNA groove binding or partially intercalating molecules cause little or no effect on the relative viscosity of the DNA solution. Plots of the relative viscosity $(\eta/\eta_0)^{1/3}$ vs [complex]/[DNA] ratio for **2**−**6** show only a minor change in the relative specific viscosity, indicating groove or partial intercalative binding nature of the complexes to CT DNA, where η and η_0 are the specific viscosity of DNA in the presence and absence of the complex, respectively (Figure 3b). A comparison of the viscosity data with intercalator ethidium bromide and groove binder Hoechst dye indicates a partial intercalative mode of binding of the dppz complexes.

Chemical Nuclease Activity. The DNA cleavage activity of the ferrocenyl complexes **1**−**4** and **5**−**7** as controls (10 μM) was studied in the presence of hydrogen peroxide (H_2O_2, 200 μM) as an oxidizing agent and glutathione (GSH, 1 mM) and 3-mercaptopropionic acid (MPA, 200 μM) as reducing agents using supercoiled pUC19 DNA (0.2 μg, 30 μM) in 50 mM Tris−HCl/50 mM NaCl buffer (pH 7.2). The extent of DNA cleavage was estimated from the gel electrophoresis diagram which is shown in Figure 4 (Figure S20, Supporting Information). The choice of both H_2O_2 and reducing agents was based on the observation of the Fc^+−Fc and Cu(II)−Cu(I) redox couples in **1**−**6** in cyclic voltammetric studies. Complexes **1**−**4** showed significant chemical nuclease activity in the presence of both oxidizing and reducing agents. Control experiments using the ferrocenyl ligand, phenanthroline bases, H_2O_2, GSH, or MPA alone did not show any apparent cleavage of CT DNA under similar experimental conditions (Figure S21, Supporting Information). The Zn(II)

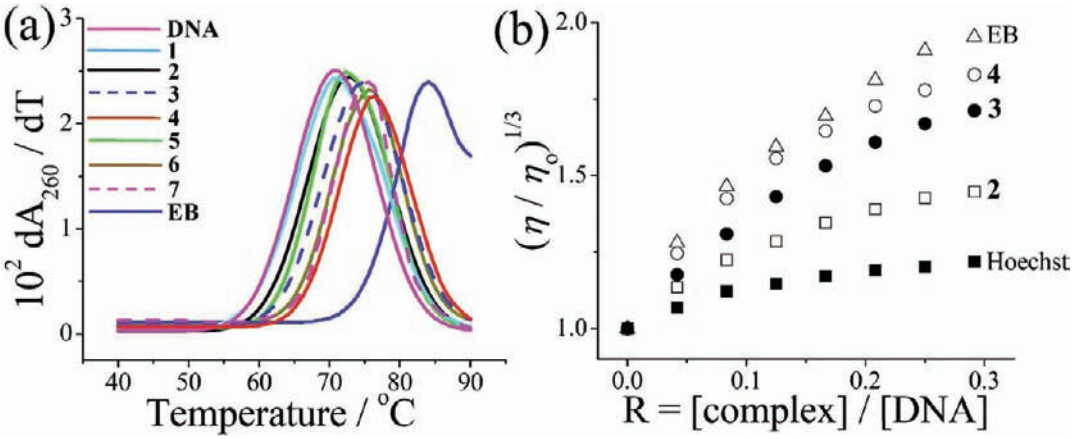

Figure 3. (a) DNA melting temperature plot using CT DNA (190 μM NP) in the absence and presence of 20 μM ethidium bromide (EB) and complexes **1**−**6** in 5 mM phosphate buffer (pH = 6.8). (b) The effect of increasing concentration of EB (Δ), Hoechst dye (■), **2** (□), **3** (●), and **4** (○) on the relative viscosity of CT DNA at 37.0(±0.1) °C in 5 mM Tris-HCl buffer (pH = 7.2, [CT DNA] = 160 μM).

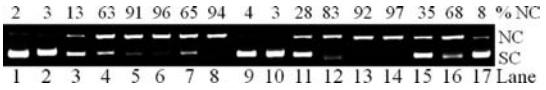

Figure 4. Gel electrophoresis diagram showing the chemical nuclease activity of complexes **1**−**7** (10 μM) using SC pUC19 DNA (0.2 μg, 30 μM b.p.) in the presence of 1.0 mM glutathione (GSH) as a reducing and 200 μM H_2O_2 as an oxidizing agent: lane 1, DNA control; lane 2, DNA + GSH; lanes 3−9, DNA + **1**−**7** + GSH, respectively; lane 10, DNA + H_2O_2; lanes 11−17, DNA + **1**−**7** + H_2O_2, respectively.

complex **7** did not show any apparent chemical nuclease activity in the presence of oxidizing or reducing agents. The chemical nuclease activity follows the order **4** (Fc-Trp-Cu-dppz) ≈ **6** (Ph-Trp-Cu-dppz) > **3** (Fc-Trp-Cu-dpq) > **2** (Fc-Trp-Cu-phen) ≈ **5** (Ph-Trp-Cu-phen). The cleavage activity seems to follow the duplex DNA binding strength of the complexes.

The mechanistic aspects of the chemical nuclease activity were studied using additives like hydroxyl radical scavengers (catalase, DMSO, KI, mannitol) or singlet oxygen quenchers (NaN_3, TEMP, L-His) (Figure S22, Supporting Information). While hydroxyl radical scavengers showed inhibition of the DNA cleavage activity of the complexes, singlet oxygen quenchers had no apparent inhibitory effect. The mechanistic data indicate the involvement of reactive hydroxyl radicals in the DNA cleavage reactions. A significant inhibition in the DNA photocleavage activity was observed under argon, suggesting the necessity of molecular oxygen to generate the reactive species (Figure S22, Supporting Information). The DNA groove binding preference of the complexes was studied using DNA major groove binder methyl green and DNA minor groove binder distamycin. A significant inhibition in the chemical nuclease activity of the phen and dpq complexes was observed in the presence of distamycin (100 μM), while methyl green (100 μM) addition has no apparent effect on the DNA cleavage of these complexes. The results indicate the minor groove binding propensity of the phen and dpq complexes. The dppz complex **4** showed inhibition in the chemical nuclease activity only in the presence of methyl green, suggesting the major groove binding nature of **4** to the duplex DNA (Figure S23, Supporting Information).

Photoinduced DNA Cleavage. The DNA cleavage activity of complexes **1**−**7** was studied using SC pUC19 DNA (30 μM, 0.2 μg) in Tris-HCl/NaCl (50 mM, pH 7.2) buffer on irradiation with monochromatic blue, green, and red light of respective 454, 568, and 647 nm wavelength (laser power =50 mW). The extent of SC DNA cleavage to its NC (nicked circular) form at these wavelengths is shown in Figure 5 (Figure S24, Supporting Information). The choice of these wavelengths was based on the presence of metal-centered bands near 450 and 600 nm for the complexes (Figure 1). The DNA photocleavage activity at 454 nm follows the order **4** (Fc-Trp-Cu-dppz) > **3** (Fc-Trp-Cu-dpq) > **6** (Ph-Trp-Cu-dppz) > **2** (Fc-Trp-Cu-phen) > **7** (Fc-Trp-Zn-dppz) > **5** (Ph-Trp-Cu-phen) > **1** (Fc-Trp-Cu-bpy). Complexes **1** and **2** are poor photocleavers of DNA since both bpy and phen are photoinactive in nature. Since 454 nm corresponds to the visible band of the ferrocenyl unit, complexes having the Fc moiety are more photoactive than those lacking this unit. This is evidenced from better photocleavage activity of **4** than **6**. In contrast, at 568 and 647 nm the activity of the complexes follows order **4** (Fc-Trp-Cu-dppz) > **3** (Fc-Trp-Cu-dpq) > **6** (Ph-Trp-Cu-dppz) > **2** (Fc-Trp-Cu-phen) > **5** (Ph-Trp-Cu-phen) > **1** (Fc-Trp-Cu-bpy) ≈ **7** (Fc-Trp-Zn-dppz). Since these wavelengths correspond to the Cu(II)-centered visible band, Cu(II) complexes **4** and **6** are more active than the Zn(II) complex **7** having dppz as the phenanthroline base. The cleavage activity follows the DNA binding trend of the complexes and the photosensitizing ability of the phenanthroline bases. The Ph-Trp complexes **5** and **6** have an axial aqua ligand. Both complexes show ∼20% cleavage of DNA in the dark in the absence of any external additives. This is due to hydrolytic cleavage of DNA. In contrast, the Fc-Trp complexes did not show any significant hydrolytic DNA cleavage activity. The control complexes without any ferrocenyl moiety showed ∼35% lower DNA photocleavage activity than the ferrocene conjugates under similar experimental conditions. The bpy complex **1** is a poor photocleaver of DNA since it lacks DNA binding ability.

The phen complex **2** (15 μM) cleaved SC DNA in blue light of 454 nm, giving ∼60% NC form. Since phen ligand does not have any photosensitizing ability, the observed photocleavage of **2** is due to the presence of a photosensitizing indole moiety in the amino acid. A 15 μM solution of **3** and **4** essentially completely nicked SC DNA at this wavelength. The complexes also cleaved DNA in green light of 568 nm. Complexes **3** and **4** (20 μM)

dx.doi.org/10.1021/ic201028e |*Inorg. Chem.* 2011, 50, 8452–8464

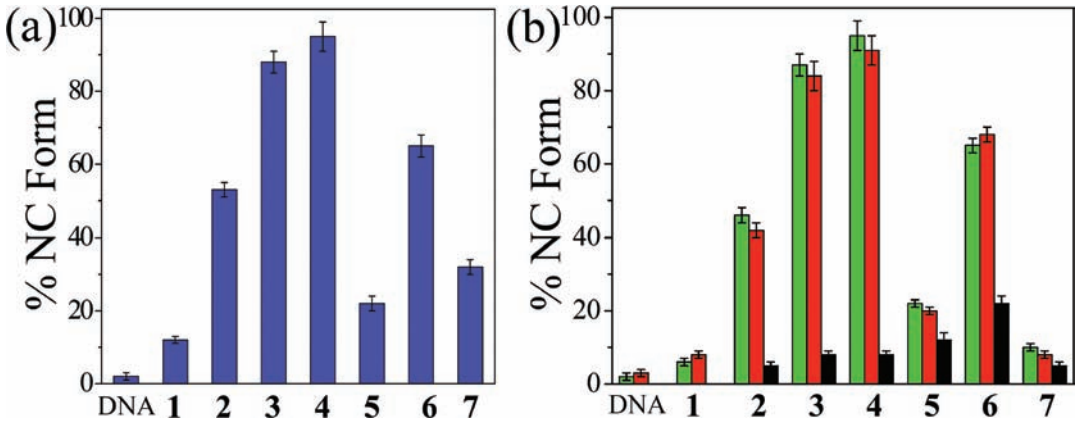

Figure 5. Bar diagram showing visible light-induced DNA cleavage activity of complexes **1**−**7** using SC pUC19 DNA (0.2 μg, 30 μM b.p.) for an exposure time of 2 h and laser power of 50 mW (color code: blue, 454 nm; green, 568 nm; red, 647 nm; black, unexposed to light).

Table 4. Selected DNA (SC pUC19, 0.5 μg) Cleavage Data for [Cu(Fc-Trp)(L)](ClO$_4$) (L = bpy, 1; phen, 2; dpq, 3; dppz, 4), [Cu(Ph-Trp)(L)(H$_2$O)](ClO$_4$) (L = phen, 5; dppz, 6), and [Zn(Fc-Trp)(dppz)](ClO$_4$) (7) in Visible Light

reaction conditions[a]	% NC form (λ = 454 nm)	% NC form (λ = 568 nm)	% NC form (λ = 647 nm)
DNA control	2	2	3
DNA + **1**	12	6	8
DNA + **2**	53	46	42
DNA + **3**	88	87	84
DNA + **4**	95	96	91
DNA + **5**	22	24	20
DNA + **6**	65	66	68
DNA + **7**	32	10	8

[a] In Tris-buffer medium (pH = 7.2). λ, Laser wavelength. Photoexposure time (t) = 2 h. Concentration of complexes **1**−**7** used for 454 nm experiments is 15 and 20 μM for other wavelengths. SC and NC are supercoiled and nicked circular forms of DNA.

showed complete cleavage of DNA in green light. Complex **2** also displayed significant DNA cleavage activity at 568 nm. We explored the DNA photocleavage activity in red light. Complexes **2**−**6** showed DNA cleavage activity in red light of 647 nm. The effect of the ferrocenyl moiety in DNA photocleavage reactions is evidenced from the significantly higher DNA cleavage activity of the Fc-Trp complex **4** than its Ph-Trp analogue **6**. While the control species suffer from the undesirable hydrolytic cleavage of DNA, the steric protection of two axial sites of the copper(II) center by the ferrocenyl and indole moieties makes complex **4** an efficient photocleaver of DNA without causing any hydrolytic damage to DNA. Control experiments using copper(II) acetate, Fc-TrpH, phen, dpq, or dppz alone did not show any apparent DNA photocleavage activity under similar reaction conditions. Selected DNA photocleavage data are given in Table 4. Further, to investigate any dual involvement of the Fe(II) and Cu(II) centers in augmenting the DNA photocleavage activity, the DNA photocleavage activity of the Zn(II) analogue (**7**) of complex **4** was studied. Zn(II), being redox inactive, is unlikely to get involved with the Fe(II) center of the ferrocenyl moiety in an electron transfer process. As expected, complex **7** showed significantly reduced DNA photocleavage activity than **4** at 454 nm. A 15 μM solution of **7** nicked only ∼32% of SC DNA to its NC form at this wavelength. Complex **7** is inactive in red light of 647 nm in the absence of any spectral band in the red light window (Figure S25, Supporting Information).

The mechanistic aspects of the DNA photocleavage reactions were explored using the dppz complex **4** and different additives in visible light of 454 and 647 nm wavelengths (Figure 6). The singlet oxygen quenchers like NaN_3, TEMP, or L-His had no apparent inhibitory effect on the cleavage activity, thus excluding the possibility of a type II singlet oxygen ($^1O_2$) pathway. The hydroxyl radical scavengers like DMSO, KI, mannitol, and catalase showed an inhibitory effect, suggesting formation of hydroxyl radical ($^{\bullet}OH$) as the cleavage active species via a photoredox pathway.[66,67] The photoinduced DNA cleavage activity is believed to be metal assisted involving the visible bands of the ferrocenyl moiety and the copper(II) center.[36,37]

Cytotoxicity Study. 3-(4,5-Dimethylthiazol-2-yl)-2,5-diphenyltetrazolium bromide (MTT) assay was done to test the ability of complexes **2**−**7** to inhibit cell growth and induce cell death upon photoexposure to visible light in HeLa (human cervical carcinoma) and MCF-7 (human breast adenocarcinoma) cancer cells (Figure 7, Figures S26−S28, Supporting Information). HeLa cells constitute a highly proliferative human cancer model. The complexes showed reduction in the viability of the HeLa cells in a dose-dependent manner. An enhancement in the cytotoxicity of the complexes was observed on photoirradiation with visible light (400−700 nm). Complexes **2**−**6** showed a more than 2.0-, 2.4-, 7.0-, 1.8-, and 1.4-fold increase in the respective cytotoxicity in HeLa cells in visible light of 400−700 nm when compared to the nonirradiated samples. No reduction in the cell viability was observed on photoexposure of the cells in the absence of the complex. Complexes were also found to be cytotoxic on MCF-7 cell lines in the dark, and an enhancement of the cytotoxicity was observed on exposure to visible light. A better cytotoxicity of the ferrocene-conjugated dppz complex (**4**) was observed in the dark in MCF-7 compared to the HeLa cells, giving an IC_{50} value of ∼3 μM. However, when photoactivated, there was a ∼5-fold enhancement in the cytotoxicity of complex **4**, giving an IC_{50} value of 650 nM. The Zn(II) complex **7** was not cytotoxic in the dark and visible light in HeLa cells. The data suggest possible involvement of the Cu(II) center in showing the cytotoxicity. Cell viability assay using control compounds showed that the ligands and the metal salt alone were nontoxic

dx.doi.org/10.1021/ic201028e |*Inorg. Chem.* 2011, 50, 8452–8464

to the cancer cells both in the dark and in visible light (Table S3, Supporting Information). The IC_{50} values of the complexes and Photofrin are listed in Table 5.[68] The dpq complex **3** was found to be less toxic than other complexes, and its nontoxic nature could be due to quick efflux reducing its cellular uptake. In summary, the ferrocenyl copper(II) complexes that showed significant PDT effect in visible light could serve as potent metal-based PDT agents. The ferrocenyl moiety showed a more positive effect toward photocytotoxity than the control species.

Caspase-Independent Apoptosis. The apoptosis-inducing activity of the complexes was studied. HeLa cells were treated with the complexes at 5 μM concentration and Z-VAD-FMK (pan caspase inhibitor) individually for 24 h followed by fixing the cells, staining with propidium iodide, and estimating the apoptotic cells (sub G1 population) by FACS analyses (Figure 8, Figure S29, Supporting Information). As seen from Figure 8, the phen complex **2** induces apoptosis in 35% of the cells in the dark, whereas in the presence of visible light the apoptotic activity is in 68% of the cells. The apoptosis is in 40% of cells in the dark for the dppz complex **4**, while in light it shows apoptotic activity in 84% of cells. The phen complex **5** induces apoptosis in 33% of cells in the dark, and the apoptotic activity is 60% of cells in light. The dppz control species **6** induces apoptosis in 37% of cells in the dark, but its apoptotic activity gets enhanced to 68% of cells, which is significantly less than its ferrocenyl analogue. These complexes also showed apoptotic activity in HeLa cells in the presence of pancaspase inhibitor, suggesting caspase-independent apoptosis in HeLa cells (Figure 8).[69]

Nuclear Staining. Treatment of the HeLa cells with complex **4** (10 μM for 4 h in the dark) results in marked changes in the nuclear morphology as determined by Hoechst 33258 and an acridine orange/ethidium bromide (AO/EB) dual nuclear staining (Figure 9).[70] A significant change in the nuclear morphology such as extensive chromatin aggregation or nuclear condensation was observed in the treated cells (Figure 9b and 9c) as compared

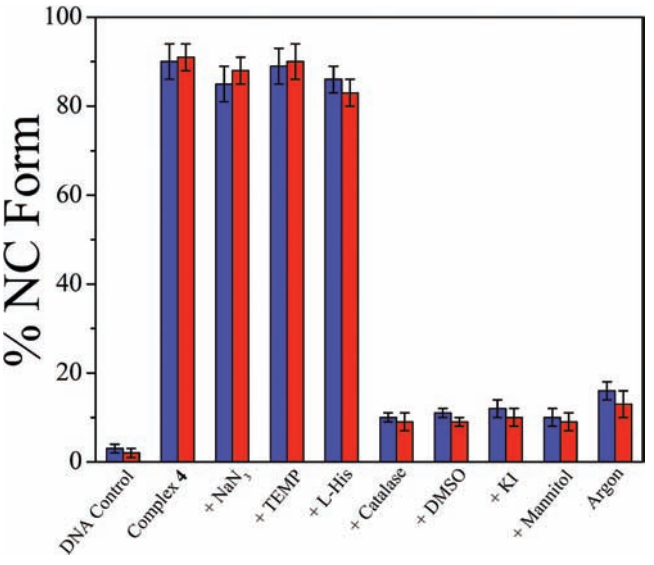

Figure 6. Bar diagram showing the mechanistic aspects of the visible light-induced DNA cleavage activity of [Cu(Fc-Trp)(dppz)](ClO$_4$) (**4**) at 454 (15 μM) and 647 nm (20 μM) using SC pUC19 DNA (0.2 μg, 30 μM b.p.) for an exposure time of 2 h (color code: blue, 454 nm; red, 647 nm).

Table 5. IC_{50} Values of Photofrin, [Cu(Fc-Trp)(L)](ClO$_4$) (L = phen, 2; dpq, 3; dppz, 4), [Cu(Ph-Trp)(L)(H$_2$O)](ClO$_4$) (L = phen, 5; dppz, 6), and [Zn(Fc-Trp)(dppz)](ClO$_4$) (7) in HeLa and MCF-7 Cells

	HeLa		MCF-7	
compound	IC_{50} (μM) dark[a]	IC_{50} (μM) visible light[b]	IC_{50} (μM) dark[a]	IC_{50} (μM) visible light[b]
2	9.57 ± 0.1	4.74 ± 0.1	4.78 ± 0.09	2.02 ± 0.07
3	24.45 ± 0.3	10.23 ± 0.3	>20	14.18 ± 0.1
4	8.95 ± 0.2	1.29 ± 0.04	2.99 ± 0.08	0.65 ± 0.03
5	8.80 ± 0.3	4.79 ± 0.2	8.74 ± 0.1	8.26 ± 0.2
6	6.10 ± 0.1	4.27 ± 0.1	4.13 ± 0.1	2.08 ± 0.09
7	>80	>80		
Photofrin[c]	>41	4.3 ± 0.2		

[a] IC_{50} values correspond to 24 h incubation in dark. Complex **7** was studied only for HeLa cells. [b] IC_{50} values correspond to 4 h incubation in the dark followed by photoexposure to visible light (400−700 nm, 10 J cm^{-2}). [c] Photofrin IC_{50} values (633 nm excitation; fluence rate 5 J cm^{-2}) are taken from ref 68 (converted to micromolar using the approximate molecular weight of Photofrin, 600 g M^{-1}).

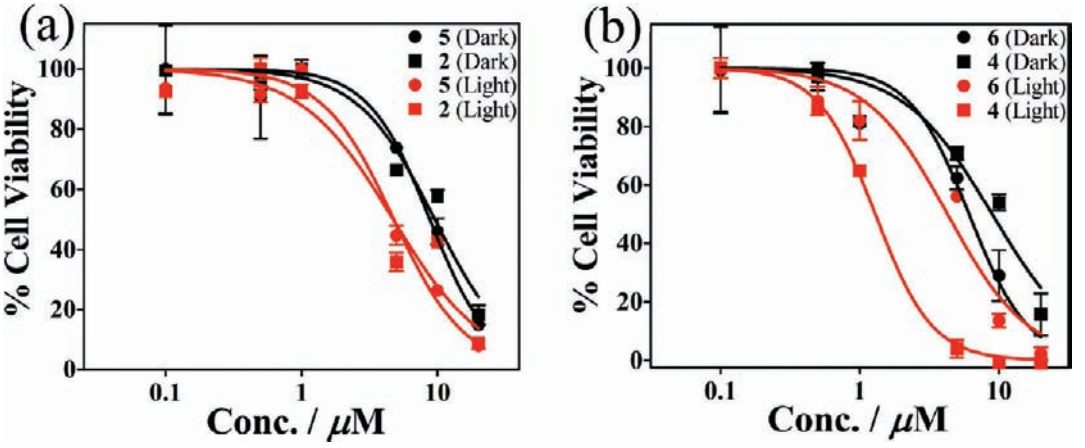

Figure 7. Cell viability plots showing the cytotoxic effect of the phen and dppz complexes (**2**, **4**, **5**, and **6**) in HeLa cells in the dark (black symbols) and in the presence of visible light (red symbols, 400−700 nm, 10 J cm^{-2}): (a) cytotoxicty of the phen complexes **2** (■) and **5** (●); (b) cytotoxicity of the dppz complexes **4** (■) and **6** (●).

dx.doi.org/10.1021/ic201028e |*Inorg. Chem.* 2011, 50, 8452–8464

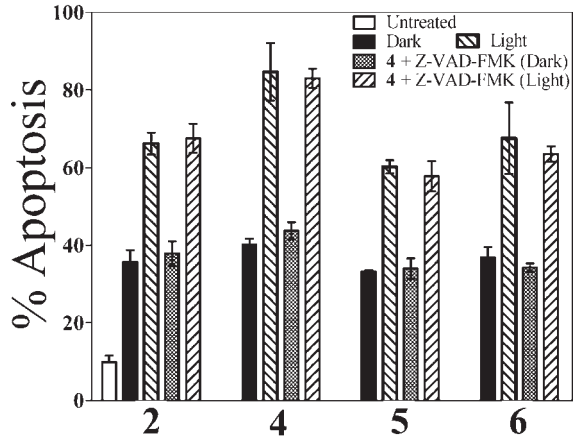

Figure 8. Bar diagram showing % apoptosis in HeLa cells induced by complexes **2**, **4**, **5**, and **6** in the dark and light (400−700 nm, 10 *J* cm^{-2}) in the presence of cell-permeable caspase inhibitor Z-VAD-FMK.

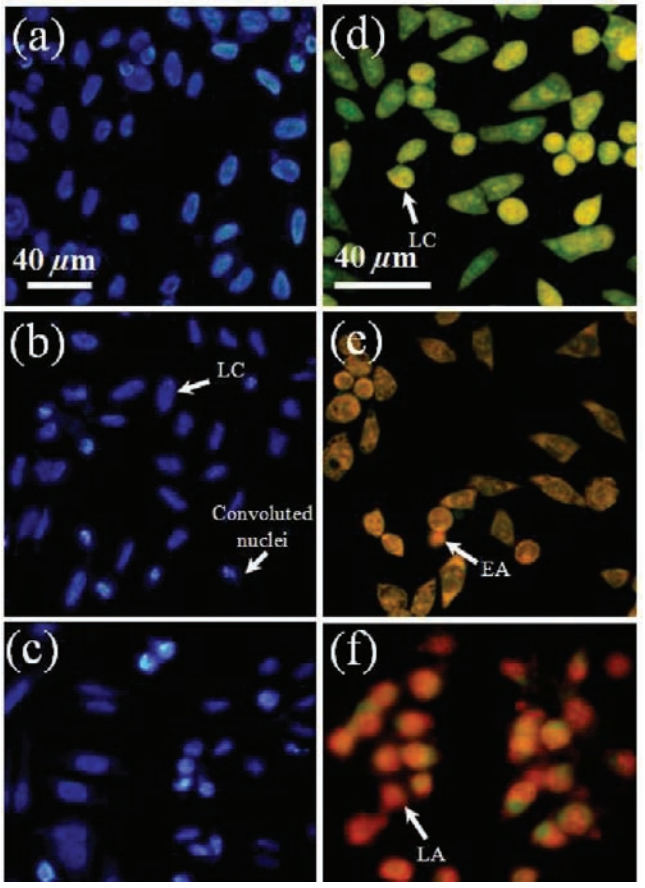

Figure 9. Hoechst 33258 and acridine orange/ethidium bromide (AO/EB) nuclear staining with complex **4** (10 μM): (a−c) Hoechst 33258 staining of HeLa cells untreated and treated with complex **4** in the dark and in the presence of visible light (400−700 nm, 10 J cm^{-2}): (a) untreated cells, (b) treated with **4** in the dark, (c) treated with **4** in the presence of light. (d−f) AO/EB dual staining of HeLa cells to identify live cell (LC), early apoptotic (EA), and late apoptotic (LA) nuclei, (d) untreated cells, (e) treated with **4** in dark, and (f) treated with **4** in the presence of light.

to the evenly stained nuclear contours of the normal HeLa cells (Figure 9a). Shrinkage in the volume of the cells and chromatin condensation suggest formation of apoptotic nuclei in the population. Significant increase in the population of apoptotic nuclei was evidenced from the Hoechst 33258 staining on irradiation with visible light for 1 h (Figure 9c). The control cells that stained evenly with this dye were also found to stain lightly and evenly with AO but stain negative for EB, indicating the presence of live cells. This can be explained from the fact that though both of these dyes intercalate to DNA, only AO can cross the plasma membrane and stain the cells while EB is actively excluded from the cells having an intact plasma membrane (Figure 9d).[54] The treated HeLa cells after 4 h of postincubation in the dark showed intensely stained orange nuclei, a characteristic of early apoptotic cells (Figure 9e). After 1 h postirradiation, the cells exhibited a condensed nucleus (red in color), which is a hallmark of late apoptotic cells (Figure 9f). The red-colored nucleus is due to the loss of membrane integrity in the late apoptotic and necrotic cells that allows EB to stain the nucleus. Nuclear staining and fluorescent microscopic images of the HeLa cells on photoexposure suggest complex-induced apoptosis that could be characterized from nuclear condensation, cell shrinkage, and surface blebbing. Apoptosis, unlike necrosis, induces minimal inflammatory response and less toxic effects to the surrounding normal tissues and hence is more tolerable to patients.

CONCLUSION

Ferrocene-conjugated L-tryptophan reduced Schiff base copper(II) complexes of phenanthroline bases were synthesized and characterized and their biological potential as photocytotoxic agents studied. The ferrocenyl complex **4** and its phenyl analogue **6** containing dipyridophenazine base show significant DNA photocleavage activity and cytotoxic property. The complexes are efficient groove binders to CT DNA, showing partial intercalative binding of the dppz complexes. The redox active complexes with quasi-reversible Fc^{+}−Fc and Cu(II)−Cu(I) couples display significant chemical nuclease activity in the presence of both oxidizing (H_2O_2) and reducing (GSH and MPA) agents involving the Fe(II) and Cu(II) center, respectively. The complexes show significant photoinduced DNA cleavage activity in visible light. Photocleavage of plasmid DNA observed in red light of 647 nm is of importance in PDT chemistry. This work makes a significant contribution to the virtually unknown chemistry of organometallic complexes as synthetic photonucleases. Evaluation of the photocytotoxic potential of the complexes in HeLa and MCF-7 cancer cells has revealed that the phen and dppz complexes are efficient PDT agents in visible light of 400−700 nm. The ferrocenyl dppz complex **4** has shown PDT activity with low dark toxicity and significant phototoxicity. Pancaspase inhibitor Z-VAD-FMK experiments have shown that these complexes induce caspase-independent apoptosis in HeLa cells. Rapid change in the nuclear morphology with Hoechst staining and acridine orange/ethidium bromide dual staining reveals that most of the HeLa cells enter early apoptosis within 1 h of light treatment. The ferrocenyl moiety shows a positive effect in the DNA photocleavage activity. Besides, the ferrocenyl moiety exhibits remarkable enhancement of the PDT effect in comparison to its control species, and our observation is akin to the positive effect reported for ferrocifen when compared to the anticancer activity of tamoxifen.[19] Bioorganometallic complexes presented in this work have essential metal ions like iron and copper, nontoxic ferrocenyl moiety, L-tryptophan amino acid, and biocompatible

phenanthroline bases. The PDT effect observed for complex **4** is remarkable in the emerging chemistry of metal-based PDT agents.

■ ASSOCIATED CONTENT

Supporting Information. CIF files giving crystallographic data for complexes **1**·H_2O and **5**, list of selected bond distance and bond angle parameters (Tables S1 and S2), cytotoxicity data (Table S3), synthetic schemes (S1−S3), and figures showing ligand spectra (S1−S4), spectral and redox plots (S5), hydrogen bonding in **1**·H_2O (S6), mass spectra of the complexes (S7−S13), absorption spectra (S14), cyclic voltammograms (S15 and S16), unit cell packing diagrams (S17 and S18), DNA binding plot (S19), gel electrophoresis and bar diagrams (S20−S25), and cellular data (S26−S29). This material is available free of charge via the Internet at http://pubs.acs.org.

■ AUTHOR INFORMATION

Corresponding Author

*Fax: 91-80-23600683. E-mail: arc@ipc.iisc.ernet.in (A.R.C.); anjali@biochem.iisc.ernet.in (A.A.K.).

■ ACKNOWLEDGMENT

We thank the Department of Science and Technology (DST), Government of India, for financial support (SR/S5/MBD-02/2007). We are thankful to DST for a CCD diffractometer facility and the Alexander von Humboldt Foundation, Germany, for donation of an electroanalytical system. T.K.G. is thankful to the Council of Scientific and Industrial Research, New Delhi, for a research fellowship. A.R.C. thanks DST for J. C. Bose national fellowship.

■ REFERENCES

(1) Hartinger, C. G.; Dyson, P. J. *Chem. Soc. Rev.* **2009**, *38*, 391–401.
(2) Fouda, M. F. R.; Abd-Elzaher, M. M.; Abdelsamaia, R. A.; Labib, A. A. *Appl. Organomet. Chem.* **2007**, *21*, 613–625.
(3) Fish, R. H.; Jaouen, G. *Organometallics* **2003**, *22*, 2166–2177.
(4) Schlawe, D.; Majdalani, A.; Velcicky, J.; Hessler, E.; Wiedler, T.; Prokop, A.; Schalz, H.-G. *Angew. Chem., Int. Ed. Engl.* **2004**, *43*, 1731–1734.
(5) Fonge, H.; Chitneni, S. K.; Lixin, J.; Vunckx, K.; Prinsen, K.; Nuyts, J.; Mortelmans, L.; Bormans, G.; Ni, Y.; Verbruggen, A. *Bioconjugate Chem.* **2007**, *18*, 1924–1934.
(6) Moriuchi, T.; Nomoto, A.; Yoshida, K.; Ogawa, A.; Hirao, T. *J. Am. Chem. Soc.* **2001**, *123*, 68–75.
(7) Top, S.; El Hafa, H.; Vessieres, A.; Huche, M.; Vaissermann, J. *Chem.—Eur. J.* **2002**, *8*, 5241–5249.
(8) Alberto, R. *Eur. J. Inorg. Chem.* **2009**, 21–31.
(9) Mucic, R. C.; Herrlein, M. K.; Mirkin, C. A.; Letsinger, R. L. *Chem. Commun.* **1996**, 555–557.
(10) Meggers, E. *Chem. Commun.* **2009**, 1001–1010.
(11) Gasser, G.; Ott, I.; Metzler-Nolte, N. *J. Med. Chem.* **2011**, *54*, 3–25.
(12) Causey, P. W.; Baird, M. C. *Organometallics* **2004**, *23*, 4486–4494.
(13) Claffey, J.; Hogan, M.; Müller-Bunz, H.; Pampillón, C.; Tacke, M. *ChemMedChem.* **2008**, *3*, 729–731.
(14) Tabbì, G.; Cassino, C.; Cavigiolio, G.; Colangelo, D.; Ghiglia, A.; Viano, I.; Osella, D. *J. Med. Chem.* **2002**, *45*, 5787–5795.
(15) Pigeon, P.; Top, S.; Vessières, A.; Huché, M.; Hillard, E. A.; Salomon, E.; Jaouen, G. *J. Med. Chem.* **2005**, *48*, 2814–2821.
(16) Anson, C. E.; Baldwin, T. J.; Creaser, C. S.; Stephenson, G. R. *Organometallics* **1996**, *15*, 1451–1456.
(17) Forrow, N. J.; Foulds, N. C.; Frew, J. E.; Law, J. T. *Bioconjugate Chem.* **2004**, *15*, 137–144.
(18) Anne, A.; Bouchardon, A.; Moiroux, J. *J. Am. Chem. Soc.* **2003**, *125*, 1112–1113.
(19) Nguyen, A.; Top, S.; Vessieres, A.; Pigeon, P.; Huche, M.; Hillard, E. A.; Jaouen, G. *J. Organomet. Chem.* **2007**, *692*, 1219–1225.
(20) Biot, C.; Glorian, G.; Maciejewski, L. A.; Brocard, J. S.; Domarle, O.; Blampain, G.; Millet, P.; Georges, A. J.; Abessolo, H.; Dive, D.; Lebibi, J. *J. Med. Chem.* **1997**, *40*, 3715–3718.
(21) Köpf, H.; Köpf-Maier, P. *Angew. Chem., Int. Ed. Engl.* **1979**, *18*, 477–488.
(22) Bergamo, A.; Sava, G. *Dalton Trans.* **2007**, 1267–1272.
(23) Yan, Y. K.; Melchart, M.; Habtemariam, A.; Sadler, P. J. *Chem. Commun.* **2005**, 4764–4776.
(24) Casini, A.; Gabbiani, C.; Sorrentino, F.; Rigobello, M. P.; Bindoli, A.; Geldbach, T. J.; Marrone, A.; Re, N.; Hartinger, C. J.; Dyson, P. J.; Messori, L. *J. Med. Chem.* **2008**, *51*, 6773–6781.
(25) Peacock, A. F. A.; Sadler, P. J. *Chem. Asian J.* **2008**, *3*, 1890–1899.
(26) Van Staveren, D. R.; Metzler-Nolte, N. *Chem. Rev.* **2004**, *104*, 5931–5985.
(27) Bonnett, R.*Chemical Aspects of Photodynamic Therapy*; Gordon & Breach: London, 2000.
(28) Sternberg, E. D.; Dolphin, D.; Brückner, C. *Tetrahedron* **1998**, *54*, 4151–4202.
(29) Henderson, B. W.; Busch, T. M.; Vaughan, L. A.; Frawley, N. P.; Babich, D.; Sosa, T. A.; Zollo, J. D.; Dee, A. S.; Cooper, M. T.; Bellnier, D. A.; Greco, W. R.; Oseroff, A. R. *Cancer Res.* **2000**, *60*, 525–529.
(30) Detty, M. R.; Gibson, S. L.; Wagner, S. J. *J. Med. Chem.* **2004**, *47*, 3897–3915.
(31) Farrer, N. J.; Salassa, L.; Sadler, P. J. *Dalton Trans.* **2009**, 10690–10701.
(32) Yam, V. W.-W.; Lo, K. K-W.; Cheung, K.-K.; Kong, R. Y.-C. *J. Chem. Soc., Dalton Trans.* **1997**, 2067–2072.
(33) Mohler, D. L.; Downs, J. R.; Hurley-Predecki, A. L.; Sallman, J. R.; Gannett, P. M.; Shi, X. *J. Org. Chem.* **2005**, *70*, 9093–9102.
(34) Herebian, D.; Sheldrick, W. S. *J. Chem. Soc., Dalton Trans.* **2002**, 966–974.
(35) Schmitt, F.; Govindaswamy, P.; Süss-Fink, G.; Ang, W. H.; Dyson, P. J.; Juillerat-Jeanneret, L.; Therrien, B. *J. Med. Chem.* **2008**, *51*, 1811–1816.
(36) Maity, B.; Roy, M.; Saha, S.; Chakravarty, A. R. *Organometallics* **2009**, *28*, 1495–1505.
(37) Maity, B.; Roy, M.; Banik, B.; Majumdar, R.; Dighe, R. R.; Chakravarty, A. R. *Organometallics* **2010**, *29*, 3632–3641.
(38) Goswami, T. K.; Roy, M.; Nethaji, M.; Chakravarty, A. R. *Organometallics* **2009**, *28*, 1992–1994.
(39) Maity, B.; Roy, M.; Chakravarty, A. R. *J. Organomet. Chem.* **2008**, *693*, 1395–1399.
(40) Perrin, D. D.; Armarego, W. L. F.; Perrin, D. R. *Purification of Laboratory Chemicals*; Pergamon Press: Oxford, 1980.
(41) Collins, J. G.; Sleeman, A. D.; Aldrich, J. R.; Greguric, I.; Hambly, T. W. *Inorg. Chem.* **1998**, *37*, 3133–3141.
(42) Amouyal, E.; Homsi, A.; Chambron, J.-C.; Sauvage, J.-P. *J. Chem. Soc., Dalton Trans.* **1990**, 1841–1845.
(43) Kahn, O. *Molecular Magnetism*; VCH: Weinheim, 1993.
(44) Walker, N.; Stuart, D. *Acta Crystallogr.* **1983**, *A39*, 158–166.
(45) Sheldrick, G. M. *SHELX-97, Programs for Crystal Structure Solution and Refinement*; University of Göttingen: Göttingen, Germany, 1997.
(46) Johnson, C. K. *ORTEP-III, Report ORNL-5138*; Oak Ridge National Laboratory: Oak Ridge, TN, 1976.
(47) Reichman, M. E.; Rice, S. A.; Thomas, C. A.; Doty, P. *J. Am. Chem. Soc.* **1954**, *76*, 3047–3053.
(48) McGhee, J. D.; Von Hippel, P. H. *J. Mol. Biol.* **1974**, *86*, 469–489.

(49) Carter, M. T.; Rodriguez, M.; Bard, A. J. *J. Am. Chem. Soc.* **1989**, *111*, 8901–8911.
(50) Cohen, G.; Eisenberg, H. *Biopolymers* **1969**, *8*, 45–55.
(51) Ausubel, F. M.; Brent, R.; Kingston, R. E.; Moore, D. D.; Seidman, J. G.; Smith, J. A.; Struhl, K. *Current Protocols in Molecular Biology*; John Wiley & Sons: New York, 2003.
(52) Bernadou, J.; Pratviel, G.; Bennis, F.; Girardet, M.; Meunier, B. *Biochemistry* **1989**, *28*, 7268–7275.
(53) Mosmann, T. *J. Immunol. Methods* **1983**, *65*, 55–63.
(54) Roy, M.; Chakravarthi, B. V. S. K.; Jayabaskaran, C.; Karande, A. A.; Chakravarty, A. R. *Dalton Trans.* **2011**, *40*, 4855–4864.
(55) Riccardi, C.; Nicoletti, I. *Nat. Protoc.* **2006**, *1*, 1458–1461.
(56) Lee, Y. J.; Shacter, E. *J. Biol. Chem.* **1999**, *274*, 19792–19798.
(57) Coligan, J. E.; Kruisbeck, A. M.; Margulies, D. H.; Shevach, E. M.; Strober, W. In *Related Isolation Procedures and Functional Assay, Current Protocols in Immunology*; Coico, R., Ed.; John Wiley & Sons, Inc.: New York, 1995; p 3.17.1.
(58) Nakamoto, K. *Infrared and Raman Spectra of Inorganic and Coordination compounds*, 4th ed.; John Wiley and Sons: New York, 1986.
(59) Sohn, Y. S.; Hendrickson, D. N.; Gray, H. B. *J. Am. Chem. Soc.* **1971**, *933*, 3603–3612.
(60) Toshima, K.; Takano, R.; Ozawa, T.; Matsumura, S. *Chem. Commun.* **2002**, 212–213.
(61) Addison, A. W.; Rao, T. N.; Reedijk, J.; Van Rijn, J.; Verschoor, G. C. *J. Chem. Soc., Dalton Trans.* **1984**, 1349–1356.
(62) Pyle, A. M.; Rehmann, J. P.; Meshoyrer, R.; Kumar, C. V.; Turro, N. J.; Barton, J. K. *J. Am. Chem. Soc.* **1989**, *111*, 3051–3058.
(63) Angeles-Boza, A. M.; Bradley, P. M.; Fu, P. K.-L.; Wicke, S. E.; Bacsa, J.; Dunbar, K. R.; Turro, C. *Inorg. Chem.* **2004**, *43*, 8510–8519.
(64) Cory, M.; Mckee, D. D.; Kagan, J.; Henry, D. W.; Miller, J. A. *J. Am. Chem. Soc.* **1985**, *107*, 2528–2536.
(65) Reinert, K. E. *Biochim. Biophys. Acta* **1973**, *319*, 135–139.
(66) Burrows, C. J.; Muller, J. G. *Chem. Rev.* **1998**, *98*, 1109–1151.
(67) Dhar, S.; Senapati, D.; Reddy, P. A. N.; Das, P. K.; Chakravarty, A. R. *Chem. Commun.* **2003**, 2452–2453.
(68) Delaey, E.; Van Laar, F.; De Vos, D.; Kamuhabwa, A.; Jacobs, P.; De Witte, P. *J. Photochem. Photobiol., B* **2000**, *55*, 27–36.
(69) Shih, C.-M.; Wu, J.-S.; Ko, W.-C.; Wang, L.-F.; Wei, Y.-H.; Liang, H.-F.; Chen, Y.-C.; Chen, C.-T. *J. Cell. Biochem.* **2003**, *89*, 335–347.
(70) Darío Díaz, G.; Paraskeva, C.; Thomas, M. G.; Binderup, L.; Hague, A. *Cancer Res.* **2000**, *60*, 2304–2312.